ACCOUNTS
of chemical research

Ultrafast Nonlinear Coherent Vibrational Sum-Frequency Spectroscopy Methods To Study Thermal Conductance of Molecules at Interfaces

JEFFREY A. CARTER, ZHAOHUI WANG, AND DANA D. DLOTT*

*School of Chemical Sciences, University of Illinois at Urbana–Champaign,
Chemical and Life Sciences Laboratory, 600 South Mathews Avenue,
Urbana, Illinois 61801*

CONSPECTUS

It is difficult to study molecules at surfaces or interfaces because the total number of molecules is small, and this is especially problematic in studies of interfacial molecular dynamics with high time resolution. Vibrational sum-frequency generation (SFG) spectroscopy, where infrared (IR) and visible pulses are combined at an interface, has emerged as a powerful method to probe interfacial molecular dynamics. The nonlinear coherent nature of SFG helps overcome the sensitivity issues, especially when femtosecond IR pulses are used. With femtosecond pulses, a range of vibrational transitions can be probed simultaneously and high time resolution can be achieved. Ultrafast SFG experiments use three pulses, a pump pulse to generate nonequilibrium conditions with a pair of probe pulses, and two time delay parameters. Mapping SFG intensity as a function of the two time delays creates a two-dimensional surface, where one axis (t_1) provides information about molecular dynamics driven by the pump pulses, and the

other axis (t_2) about the dynamics of the SFG probing process. We present examples of ultrafast SFG measurements drawn from our studies of heat transport through interfacial molecules that are models for molecular wires in electronic circuits. In these flash-heating experiments, a self-assembled monolayer (SAM) of long-chain molecules adsorbed on a metal surface is subjected to a large amplitude (up to 800 K) temperature jump. Specific vibrational reporter groups on the SAM molecules probed by SFG serve as tiny ultrafast thermometers ~1.5 Å thick with a ~1 ps response time. These SFG thermometers can monitor ultrafast heat transport through the SAM molecules. By varying the lengths of the molecular wires we can tell if the heat is propagating ballistically along the chains, at constant speed, or diffusively. In our analysis of 2D SFG methods, we first describe a simpler situation where the visible probe pulse is effectively infinite in duration. This is the usual way time-resolved SFG measurements are made, and the SFG experiment then becomes a function of a single time delay, the pump−IR probe delay t_1. Unfortunately, in this case the SFG signals have a large contribution from the nonresonant (NR) background generated by the metal surface, which adds a great deal of noise to the data, and the time resolution is limited by the molecule's vibrational dephasing time constant T_2, which is often 1 ps or more. We have recently shown that the NR background can be suppressed using a time delay t_2 between IR and visible probe pulses. In this now 2D SFG method, one would expect that information about the molecular response to the pump pulses would be contained in slices along the t_1 axis, but by simulating the experiment we show that the t_1 and t_2 parameters interact. Changing t_2 to suppress the NR background causes t_1 slices to shift in time. We also show how to improve the time resolution of ultrafast SFG experiments while maintaining NR suppression using femtosecond visible pulses at appropriate t_2 delay values.
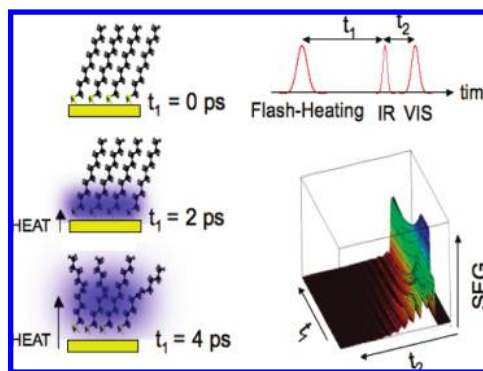
1. Introduction

Our ability to probe ultrafast dynamics of interfacial molecules has been revolutionized by vibrational sum-frequency generation (SFG) spectroscopy, where a nonlinear coherent signal is generated by combining a vibrational infrared (IR) and a "visible" pulse.[1]

(The "visible" pulse is frequently near-IR). SFG has monolayer sensitivity and interface selectivity[1] resulting from the symmetry of $\chi^{(2)}$. In the dipole approximation, SFG can be viewed as coherent IR excitation plus anti-Stokes Raman scattering. In centrosymmetric media only surface or interfacial mol-

ecules generate sum-frequency. SFG is has become a ubiquitous powerful tool in surface chemistry, as illustrated by applications to polymer surfaces[2] and buried interfaces[3] such as water−air[4] or electrochemical interfaces.[5]

Two notable advances in SFG are broadband multiplex SFG,[6−8] where a femtosecond broadband IR (BBIR) pulse is combined with a narrowband visible pulse to probe multiple vibrational transitions simultaneously, and nonresonant suppression[9] of the nonresonant (NR) background that plagues all nonlinear spectroscopies,[10] but which is particularly problematic for adsorbates on metal surfaces.[11]

Ultrafast SFG was used to study adsorbate dynamics such as diatomic-molecule desorption from metals,[12,13] energy transfer among adsorbates,[14−16] and hydrogen bond dynamics at water−air and water−lipid interfaces.[17,18] In our laboratory, SFG has been used to probe the response of self-assembled monolayers (SAMs) to laser-generated shock waves[19,20] or large-amplitude temperature jumps (T-jump).[21] SFG from vibrational reporters at known locations in the SAM make it possible to watch vibrational energy move over atomic-scale distances in real time.[22] For instance we showed we can input vibrational energy to one location of a substituted aromatic SAM and probe its arrival from two other locations.[23]

An ultrafast SFG pump−probe experiment uses three pulses, a pump pulse and a probe IR and visible pulse pair, so the experiment can be represented by a 2D surface with two delay time parameters t_1 and t_2. t_1 is the pump−IR delay, and t_2 is the IR−visible delay. (All time parameters are defined in Table 1.) Slices along t_1 provide information about interfacial molecular response to pump pulses. Slices along t_2 provide information about interfacial vibrational dynamics. However we will see these variables are interdependent.

We now describe measurements combining SFG with laser flash-heating to probe vibrational energy in interfacial molecules.[21,24] Although an oversimplification, we will for convenience[21,24] describe this as "heat flow". The SFG methods described here share many similarities (but not interface selectivity) with femtosecond stimulated Raman probe methods,[25] since both employ femtosecond broadband and picosecond narrowband pulses.

2. Time-Resolved Flash-Thermal Molecular Conductance

Our ultrafast flash-thermal molecular conductance method[21,24] is described in Figure 1. A femtosecond flash-heating pulse from the back side (opposite the SAM) of a 50 nm thick polycrystalline Au(111) layer creates a large-ampli-
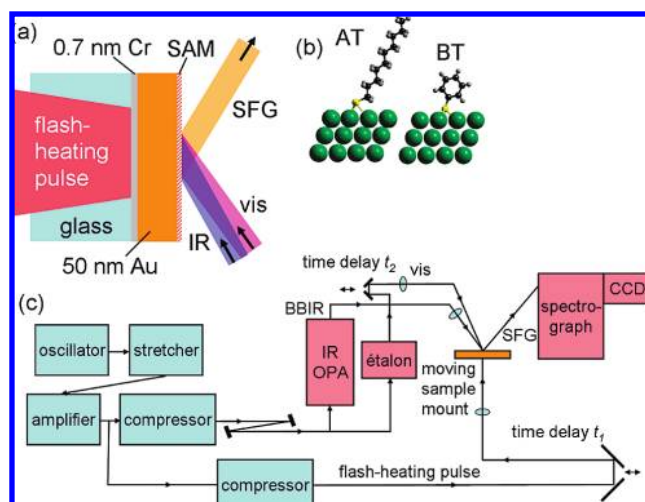

FIGURE 1. Ultrafast flash-heating molecular thermal conductance. (a) A femtosecond pulse flash-heats an Au layer from the back. Heat flow from Au to the self-assembled monolayer (SAM) molecules on the front is probed by vibrational sum-frequency generation (SFG). (b) Structure of single alkanethiol (AT) and benzenethiol (BT) molecules on Au. Actual experiments probe regions with ~10^{11} molecules. (c) Laser apparatus schematic. OPA = optical parametric amplifier with difference-frequency generation. With the étalon in place, the visible (vis) is a time-asymmetric picosecond narrow-band NBVIS pulse. With the étalon removed it is a femtosecond visible FSVIS pulse. Adapted with permission from ref 23. Copyright 2008 American Chemical Society.

TABLE 1. Lexicon of Time Parameters

t_1	delay time between flash-heating and BBIR pulses
t_2	delay time between BBIR and visible pulses
T_2	molecular vibration dephasing time constant
t_0	time for heat burst to propagate along alkanethiol (AT) chains
τ	time for AT chains to equilibrate with hot metal surface

tude T-jump ΔT up to 800 K. This large ΔT generates chemically significant heat flow[21,24] and mimics dissipation processes in molecular electronics.[21,24,26−28] Back-side heating ensures the SAMs do not see an intense electric field. Initially alkanethiol (AT) SAMs with structures $-S-(CH_2)_n-CH_3$ (Figure 1b) where n was an odd number between 5 and 23 were studied.[21] In AT SAMs, SFG selectively probes terminal methyl groups. The methylene lattice is centrosymmetric and generates minimal SFG.[19,21] Heat flowed from Au to the thiolate link, along AT chains until it reached the methyl groups.[11,29] Subsequently we studied aromatic SAMs including benzenethiol (BT) $-S-(C_6H_5)$ (Figure 1b).[23,24]

The laser apparatus[23] is depicted in Figure 1c. A Ti:sapphire laser produced 3 mJ, 800 nm, 120 fs pulses. The output was split into a visible pulse and a pump pulse for an optical parametric amplifier producing 300 fs BBIR pulses. The flash-heating pulse duration was in the 600 fs range to minimize flash-heating intensity without degrading time resolution. This variable

duration pulse was generated from the 120 ps amplifier output prior to compression in an auxiliary compressor.

The visible pulse could be transmitted through a Fabry–Perot étalon with a 5 μm air gap to create a picosecond narrow-band pulse with a nearly Lorentzian spectrum with fwhm $\sim$10 cm^{-1}. Generated by the ring-down of the femtosecond pulse in the Fabry–Perot cavity, it is nearly a single-sided exponential,[9] having a 300 fs rise and a 1 ps exponential fall time constant.

3. Time Domain Picture of SFG

SFG spectroscopy is usually described in the frequency-domain.[10,30] IR and visible pulses interact via $\chi^{(2)}$ to generate an SFG polarization with a resonant R part from molecular vibrations and a nonresonant NR part,[30,31]

$$I_{SFG}(\omega) \propto |P_{SFG}(\omega)|^2 = |P_R(\omega) + P_{NR}(\omega)|^2$$
$$= |[\chi_R^{(2)}(\omega) + \chi_{NR}^{(2)}(\omega)]E_{IR}E_{vis}|^2 \quad (1)$$

In eq 1, $\chi^{(2)}$ is a third-rank tensor. In terms of molecular hyperpolarizability β and number density N,

$$\chi_{ijk,R}^{(2)} = N \sum_{abc} \langle (i \cdot a)(j \cdot b)(k \cdot c) \rangle \beta_{abc} \quad (2)$$

where $(i \cdot a)$ is the projection of molecular axis a on laboratory-frame axis i and $\langle ... \rangle$ is orientational average.

A time-domain picture is useful for ultrafast experiments.[21,32] The SFG signal is described by a second-order response function $R^{(2)}(t, t_2)$,[33]

$$P_i^{(2)}(t, t_2) = \int_{-\infty}^{\infty} \int_{-\infty}^{\infty} R_{ijk}^{(2)}(t, t_2) E_{j,VIS}(t - t_2 - \tau_2) \times$$
$$E_{k,IR}(t - \tau_1) \, d\tau_1 \, d\tau_2 \quad (3)$$

where $P_i^{(2)}$ is the ith component of the polarization, and t_2 the time delay between IR and visible pulses. For pump–probe SFG experiments, the response function $R^{(2)}(t, t_1, t_2)$ and polarization $P^{(2)}(t, t_1, t_2)$ now depend on the pump–IR delay t_1. The SFG spectrum is

$$I_{SFG}(\omega, t_1, t_2) \propto |\int_{-\infty}^{\infty} P^{(2)}(t, t_1, t_2) \, e^{-i\omega t} \, dt|^2 \quad (4)$$

The pulse timing diagram for flash-heating SFG is depicted in Figure 2. The BBIR pulse arrives at $t = 0$, the flash-heating pulse at $-t_1$ and the visible pulse at t_2. As shown in Figure 2a,b, with femtosecond visible pulses t_2 is measured from the pulse peak. With narrow-band visible pulses t_2 is measured from halfway up the rising edge. In Figure 1c, the BBIR pulse arriving at $t = 0$ creates coherent first-order polarizations $P_{NR}^{(1)}(t)$ and $P_R^{(1)}(t)$ which undergo free-induction decays (FIDs) and radiate in the IR. The decay of $P_{NR}^{(1)}(t)$, originating mainly from metal surface electronic

transitions, is so fast that $P_{NR}^{(1)}(t)$ exists only during the BBIR pulse. $P_R^{(1)}(t)$ originates from molecular vibrations. Each transition within the BBIR bandwidth decays with its characteristic time constant $T_2 = (\pi c \Delta \nu)^{-1}$, where $\Delta \nu$ is the vibrational line width. For typical SAMs, T_2's are frequently $\sim$1 ps ($\Delta \nu \sim 10$ cm^{-1}) but there are exceptions such as ultrabroad hydrogen-bonded transitions.[4,17] When $P^{(1)}$ is combined with a visible field, the sum frequency can be generated, but only from noncentrosymmetric media. The SFG pulse is detected by a spectrograph and multichannel array.

In broadband multiplex SFG,[6] the narrow-band visible pulse is usually generated by spectral filtering of a femtosecond visible pulse to create a time-symmetric pulse, generating spectra such as the one in Figure 3b from an AT SAM. The broader feature is the NR signal from $P_{NR}^{(1)}(t)$, whose spectrum tracks the BBIR pulse spectrum. The three sharper dips are CH-stretch transitions of the AT terminal methyl groups arising from $P_R^{(1)}(t)$. In Figure 3b, the methylene transitions are present only weakly. In order to observe an intrinsic rather than instrument-limited vibrational line width $\Delta \nu$, the narrow-band visible pulse duration should be effectively infinite in duration, meaning the visible pulse duration greatly exceeds the FID duration. Then the SFG output pulse would track the FID and persist for a few multiples of T_2.[32] In Figure 3a the vibrational transitions appear as dips because $P_{NR}^{(1)}(t)$ and $P_R^{(1)}(t)$ are $\sim$180° out-of-phase. The phase difference is not always 180°;[34] it depends on a number of factors including type of metal surface, visible wavelength and molecular orientation.
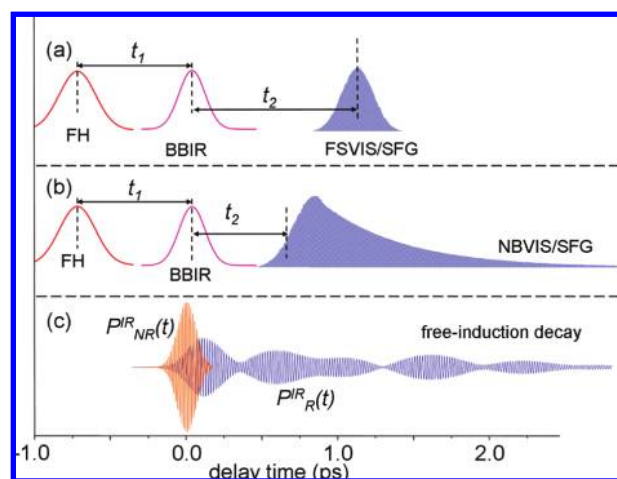

FIGURE 2. Pulse timing diagrams. The broadband femtosecond infrared (BBIR) pulse arrives at $t = 0$ and the flash-heating (FH) pulse at $-t_1$. (a) The delay of the femtosecond visible pulse (FSVIS) or (b) the time-asymmetric narrowband picosecond (NBVIS) pulse is t_2. SFG signals can be emitted only when visible pulses (shaded regions) are present. (c) Free-induction decay (FID) generated by the BBIR pulse consists of a faster $P^{IR}_{NR}(t)$ from the nonresonant (NR) susceptibility, and a slower $P^{IR}_R(t)$ from molecular vibrational resonances (R).
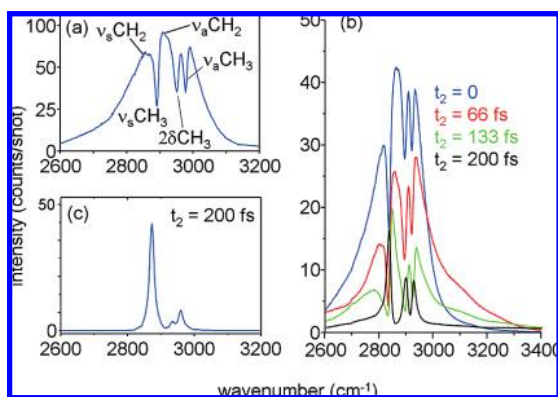
FIGURE 3. (a) Broadband multiplex SFG spectrum of 18-carbon alkanethiol (AT) SAM on Au without nonresonant (NR) suppression. (b) AT SAM spectrum using a time-delayed time-asymmetric NBVIS pulse. As the BBIR−NBVIS delay time t_2 is increased, the NR contribution disappears. (c) Fully NR suppressed spectrum of AT SAM. Adapted with permission from ref 9. Copyright 2007 American Chemical Society.

When a femtosecond visible pulse is used,[30,35,36] as in Figure 2a, the SFG emission will be a femtosecond-duration burst, so high temporal resolution is achieved at the expense of poor spectral resolution limited by the visible pulse bandwidth not T_2. For shorter values of t_2, the SFG signal has both R and NR parts. When the femtosecond visible pulse is delayed beyond $P_{NR}^{(1)}(t)$, the NR is suppressed. Spectra obtained in this manner with an AT SAM on Au(111) are shown in Figure 4. Figure 4b shows a poorly resolved spectrum versus t_2, and Figure 4c shows wavelength-integrated intensities versus t_2, which track the FID modulation envelope.[36] With varying t_2 the three CH-stretch transitions vary in prominence,[36] and it seems impossible to selectively observe just one.

With time-asymmetric narrow-band visible pulses, as in Figure 2b, SFG spectra can be obtained with any desired resolution, but the NR contribution can be suppressed by setting t_2 just beyond $P_{NR}^{(1)}(t)$.[9] Figure 3a shows a series of such spectra versus t_2 from an AT SAM on Au(111).[9] As t_2 is increased, the vibrational resonances evolve from dips to peaks, eventually yielding the deeply NR suppressed spectrum[9] in Figure 3c.

Using eq 1 we will model the SFG spectrum for a single Lorentzian line centered at frequency ω_0 against a frequency-independent NR background and note that for multiple transitions, simply add up more Lorentzian terms, unless they are overlapping in which case each may have its own phase. In reality SAM transitions may have some inhomogeneous broadening and a Voigt profile may be more realistic, but the physics described here will remain the same. We will express the BBIR spectrum as a Gaussian centered at ω_{IR}^L with spectral width $\delta\omega_L$,[34,37] and $\delta\omega_L$ is typically 200−250 cm^{-1}. Then,

$$I_{SFG}(\omega + \omega_{VIS}) \propto \exp\left[-\frac{(\omega - \omega_{IR}^L)^2}{2(\delta\omega_L)^2}\right] \times \left| A_{NR}\, e^{i\psi_{NR}} + N\frac{A_R}{\omega - \omega_0 + i\Gamma} \right|^2$$

$$= \exp\left[-\frac{(\omega - \omega_{IR}^L)^2}{2(\delta\omega_L)^2}\right] \times \left\{ A_{NR}^2 + \frac{N^2 A_R^{\,2}}{(\omega - \omega_0)^2 - \Gamma^2} + 2\frac{A_{NR}N A_R}{\sqrt{(\omega - \omega_0)^2 - \Gamma^2}}\cos(\Delta\psi) \right\} \quad (5)$$

where ω_0 is the vibrational transition center frequency, Γ is the line width (damping parameter), $\Delta\psi$ is the relative phase, and A_{NR} and A_R are amplitude factors for the NR and R contributions.

In time-resolved SFG, the focus is generally on determining the molecular response to the pump pulses as a function of delay time t_1. The pump pulses can create a time-varying R contribution by causing either N or A_R to vary with time. For instance in flash-desorption, N decreases with time as molecules leave the surface while A_R stays approximately constant. In our flash-heating experiments N stays constant but A_R decreases with time as the SAMs become thermally disordered.[21,24] A_R contains time-dependent ensemble-averaged orientation factors hidden in the response function $R^{(2)}$, similar to the frequency-domain factors in eq 2.

However owing to interference between R and NR terms, any time-dependence of the NR signal will modulate the R signal as well. It is now possible to avoid this issue by NR suppression with a visible pulse delayed by t_2, but we will show below that in this case the t_1 dependence of the SFG signal is affected by the value of t_2. Even when the NR is time-independent, the t_1-dependence of the R signal can be affected by the presence or absence of NR. When the NR signal dominates ($\chi_{NR} \gg \chi_R$) as in Figures 3a and 6, SFG resonances appear via the cross term $2\chi_{NR}^{(2)}\chi_R^{(2)}\cos(\Delta\psi)$, the R contribution is linear in χ_R, and $I_{SFG}(t) \propto N(t)A_R(t)$. When $\chi_{NR} \ll \chi_R$, which occurs with NR suppression, $I_{SFG}(t) \propto [N(t)\, A_R(t)]^2$. In intermediate cases where χ_R is comparable to χ_{NR}, the time-variation of χ_R against a constant χ_{NR} has both linear and quadratic dependences on $N(t)\, A_R(t)$.[9,34]

4. Flash Heating and Molecular Heat Conductances

Femtosecond heating of Au thin films is well-understood when ΔT is small,[38] ≤10 K, but remains incompletely understood for ΔT up to or beyond the melting point. A flash-heating pulse generates hot electrons in the first 15 nm of the Au layer. In the
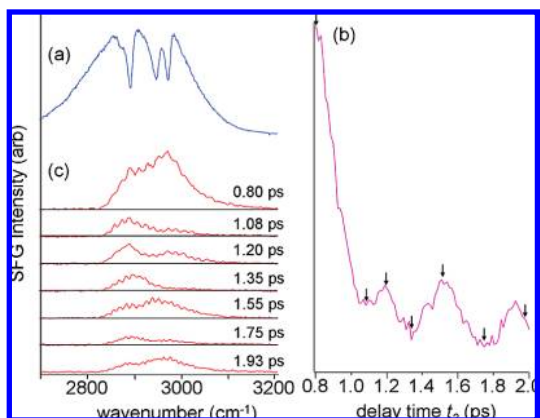
FIGURE 4. (a) SFG reference spectrum of alkanethiol SAM with NBVIS probe pulses and nonresonant background present, showing three methyl CH-stretch transitions (sharper dips). (b) Free-induction decay (FID) using a broadband femtosecond visible (FSVIS) pulse obtained by detecting the wavelength-integrated SFG signal versus delay time t_2. (c) SFG spectra with FSVIS pulses at values of t_2 indicated by arrows in (b).
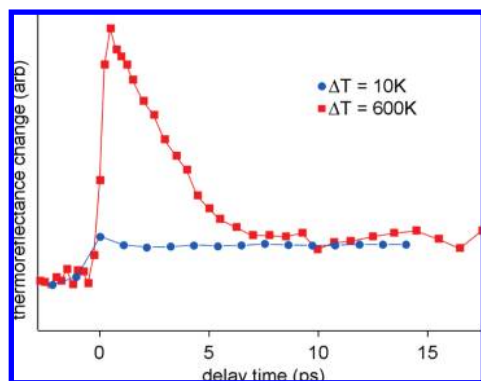

FIGURE 5. Femtosecond heating of Au thin film probed by time-resolved thermoreflectance. With smaller $\Delta T = 10$ K, the hot electrons and the lattice equilibrate within ~1 ps. With larger $\Delta T = 600$ K the lattice equilibrates within ~6 ps.

usual two-temperature model,[38,39] the initial electron temperature T_e is greater, sometimes 100 times greater, than ΔT since electronic heat capacities are small. Au hot electrons have a high diffusion coefficient, so they can quickly transport heat from the back to the front of a 50 nm thick layer. These electrons cool on the picosecond time scale by heating the Au lattice until an equilibrium ΔT is reached. The Au reflectance is sensitive to T_e, and in our initial characterizations of flash-heating, we used a thermoreflectance apparatus[21,24,40] that monitored the Au front and back surfaces with weak flash-heating pulses. As shown in Figure 5, the Au layer reached 80% of the final temperature in 1 ps and equilibrated in 5 ps. To better understand large-amplitude T-jump, we developed a new thermoreflectance apparatus that probes Au with a white-light continuum encompassing the interband transition[41] near 540 nm. Interband transitions are more sensitive to T_e than 400 or 800 nm probes used previ-
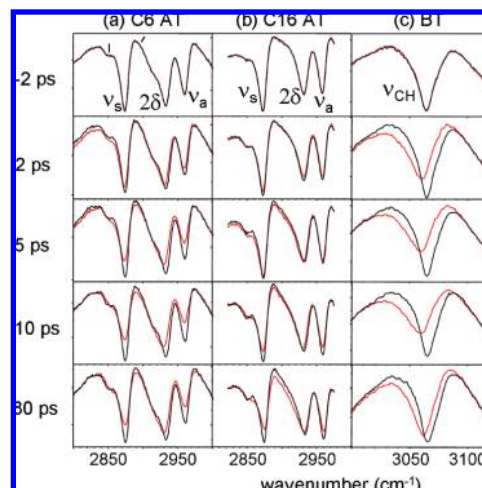

FIGURE 6. SFG spectra with NR signal present, obtained with shorter (C6) and longer (C16) alkanethiol (AT) SAMs and with benzenethiol (BT). The black curves are ambient temperature reference spectra and the red were obtained after flash-heating at the indicated times. With the AT SAM, flash heating causes the three methyl transitions (dips) to become shallower. Heat reaches the terminal methyl groups of the AT SAMs more quickly when the chains are shorter. With BT, flash heating causes the single dip to become shallower, broaden and redshift. Adapted with permission from ref 24. Copyright 2008 Elsevier.

ously. A recent result in Figure 5, where $\Delta T \approx 800$ K, shows that the equilibration time constant is ~2.5 ps when ΔT is large. Such an increase in the thermalization time has been predicted recently.[42]
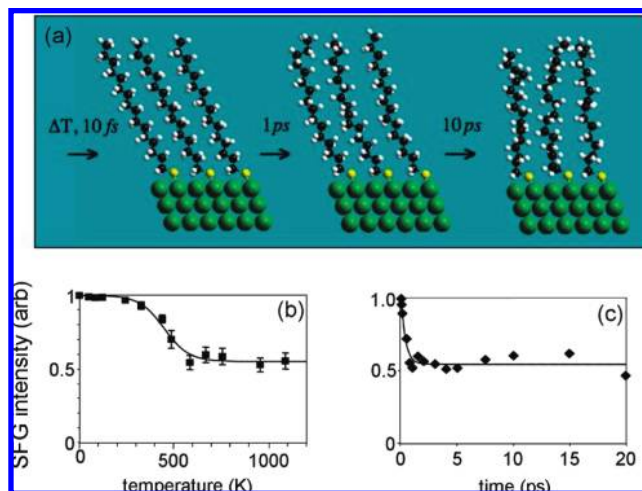

FIGURE 7. Results of molecular simulations of AT SAMs. (a) Ambient temperature structure of 16-carbon AT SAM. Simulations were performed on a unit cell of 27 AT molecules with periodic boundary conditions. When T was jumped to 1100 K, the terminal methyl groups became orientationally disordered. (b) The SFG intensity for the $\nu_s CH_3$ transition is temperature-dependent with a nearly linear response in the 300−600 K range. C. With an instantaneous temperature jump to 1100 K, the methyl head groups become orientationally disordered in ~1 ps. Adapted with permission from ref 21. Copyright 2007 AAAS.

As heat flows from the Au surface through the SAM molecules to the molecular reporter groups observed by SFG, we generally see SFG signal loss and sometimes peak broadening and peak shifting,[24] as illustrated in Figure 6. We use the *intensity loss* as a convenient "SFG thermometer".[21] To better understand SFG thermometry, we performed simulations[21] on an AT SAM unit cell with periodic boundary conditions, as shown in Figure 7. When a simulated AT SAM was heated to 1100 K, the SAM molecules became conformationally disordered (Figure 7a), causing SFG signals from $\nu_s CH_3$ of the initially well-aligned methyl groups to decrease due to a decrease in A_R. The computed loss of SFG intensity as a function of temperature (Figure 7b) is a nearly linear function of T in the 300−600 K range. To characterize the time response of the SFG thermometer, we froze all the atoms, heated the molecules to 1100 K, and released them. We observed a response time of ∼1 ps (Figure 7c). Our simulations thus indicate that the methyl groups of AT SAMs can function as tiny (1.5 Å thick) ultrafast (1 ps) thermometers.[21,23,24]

To characterize the SFG response to flash-heating we defined a vibrational response function (VRF),[19−21]

$$VRF(t) = [I(T_{cold}) - I(t)] / [I(T_{cold}) - I(T_{hot})] \qquad (6)$$

where intensities represent the depths of dips or heights of resonant peaks of vibrational transitions in the SFG spectra, $I(T_{cold})$ is the intensity at ambient temperature and $I(T_{hot})$ the intensity when Au and SAM have equilibrated after the T-jump. Figure 8 shows measured VRFs for BT and an AT SAM having 16 carbon atoms. These VRFs were extracted from streams of time-depende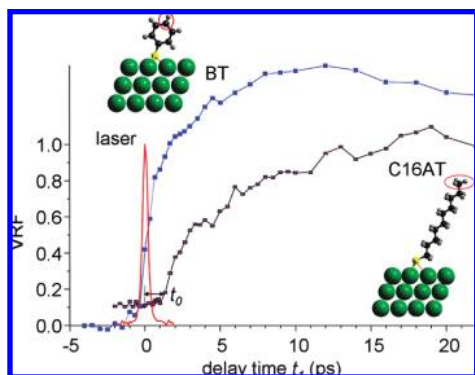nt SFG spectra such as those shown in Figure 6. In these particular studies the SFG spectra were obtained without NR suppression, so the t_2 time delay is not present.

For AT molecules, two time constants t_0 and τ were needed to characterize the time dependence of the VRF.[21] τ describes the exponential approach to equilibrium and characterizes the rate of heat flow across the Au−SAM interface.[21,24] t_0 characterizes the time delay between the flash-heating pulse and the arrival of the leading edge of the heat burst at the vibrational reporter group used for SFG thermometry, and t_0 was determined from the time the VRF first started to rise off the baseline. In AT SAMs t_0 was interpreted[21] as the time for heat to propagate along the AT chains. We observed that t_0 increased linearly with AT chain length, concluding the heat burst propagated ballistically along the chains.[21]

In the VRFs in Figure 8, obtained without NR suppression, the condition $\chi_{NR} > \chi_R$ was met, so SFG intensity loss is a linear function of A_R. Although this situation is the easiest to analyze, there is a practical downside. Fluctuations in the large NR background are the most significant source of noise in the VRF. The use of NR-suppression techniques would be expected to provide a significant improvement in signal quality.[23] Recently we have experimented with 2D NR-suppression methods using both with time-asymmetric narrow-band visible pulses and femtosecond visible pulses. Prior to presenting those data we first describe some simulations of 2D methods to assist our interpretation.

5. 2D SFG Probe Simulations

In this section we present simulations of 2D SFG with either time-asymmetric narrow-band visible pulses or femtosecond visible pulses. The simulation details will be discussed in a future publication, with a summary here:

The flash-heating pulse arriving at time $-t_1$ was 150 fs. To simulate thermal disordering, the heating pulse causes A_R to decay exponentially in time with zero onset delay ($t_0 = 0$). The time constant for thermal disordering $\tau = 2.5$ ps. The BBIR pulse at $t = 0$ is 300 fs. The FID combines $P_{NR}^{(1)}(t)$ existing only during the BBIR pulse with $P_R^{(1)}(t)$ having phase-angle $\psi = \pi$, and decay time constant T_2. The NR and R contributions have comparable amplitudes. The visible pulse arriving at time t_2 was 150 fs for the femtosecond pulse, and the narrow-band visible pulse had a 300 fs rise and a 1 ps exponential decay. The displayed 2D plots in Figures 9 and 10 show total (wavenumber-integrated) SFG intensity versus t_1 and t_2.

The simulations in Figure 9 were intended to represent a BT SAM with a single R transition with $T_2 = 1.5$ ps ($\Delta\nu = 16$ cm^{-1}). The simulations in Figure 10 were intended to repre-

FIGURE 8. Vibrational response functions (VRF) for benzenethiol (BT) and 16-carbon alkanethiol (AT) SAMs after flash-heating to ∼800 °C. The C16 data were vertically offset by +0.1 for clarity. The curve denoted "laser" is the apparatus response, and the circled structures are the vibrational reporter groups probed by SFG. The VRF of the AT SAM rises exponentially to a new equilibrium after flash-heating. There is a delay time t_0 prior to this rise resulting from the heat burst propagation along the alkane chains.
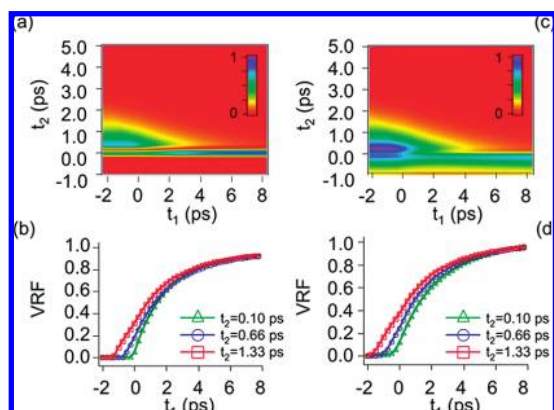
FIGURE 9. Simulated 2D SFG signals (wavelength integrated intensities) for a single oscillator against a nonresonant background using either femtosecond or picosecond pulses. The t_1 axis is the delay between the flash-heating and pulses. The t_2 axis is the delay between the BBIR and visible pulses. (b), (d) VRFs obtained from slices along the t_1 axis for indicated values of t_2.
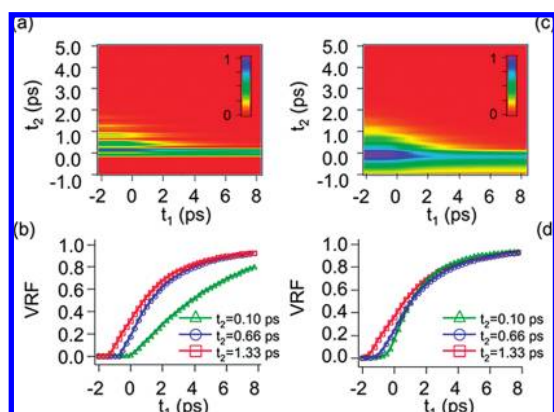

FIGURE 10. Simulated 2D SFG signals (wavelength integrated intensities) for three oscillators against a nonresonant background using femtosecond or picosecond pulses. (b), (d) VRFs obtained from slices along the t_1 axis for indicated values of t_2.

sent an AT SAM with three transitions having intensities and linewidths needed to approximate the spectrum Figure 3a.

The flash-heating response of the SAMs is nominally represented by slices of the 2D surfaces along t_1. Here we focus on what would be needed to extract the input $\tau = 2.5$ ps and $t_0 = 0$ from such slices. It might be helpful now to look once again at the AT SAM data in Figure 8 having no NR suppression. On a semilog plot, the onset delay $t_0 = 1.2$ ps was the instant when the VRF first rises off the baseline, and the heat-transfer time constant $\tau = 6$ ps was the best linear fit to the VRF rise.

The t_1-slices in Figures 9 and 10 are expressed as VRFs. A perhaps disturbing feature of these t_1 slices is that the time where the VRF rises off the baseline is not a constant t_0 but instead varies with t_2. This is understood from the timing diagrams in Figure 2a,b, which show the flash-heating pulse arriving at $-t_1$ but the SFG signal being emitted in a time window

near t_2. Thus effects of flash-heating will be observed only when $-t_1 \geq t_2$. With a nonzero value of t_2 to suppress NR, the point where the VRF first rises from the baseline is not t_0 but $t_0 - t_2$. This was not a problem for the interpretation of t_0 in our original AT experiments[21,24] since NR suppression was not used, but in future experiments with NR suppression, an accurate determination of t_0 will require a careful measurement of t_2 as well. Anecdotally, what actually occurred in our laboratory was that our t_0 measurements were consistent until we switched to NR suppression, when t_0 suddenly started varying wildly because we were inconsistent in setting t_2.

Two other interesting features of the t_1 slices in Figures 9 and 10: When femtosecond visible pulses were used, the initial rise off the baseline became more abrupt than with narrow-band visible (picosecond) pulses, indicating a time-resolution improvement. With femtosecond visible pulses, the SFG signals were emitted over a shorter time window. The $t_2 = 0.1$ ps time traces, where both R and NR were present, seem qualitatively different from the $t_2 = 0.66$ and $t_2 = 1.33$ ps traces where NR was suppressed, most dramatically in Figure 9b. In fact Figure 9a shows that the $t_2 = 0.1$ ps slice resulted from a time-dependent *increase* in the SFG intensity, whereas all the other slices represent time-dependent decreases in SFG intensity. (VRFs are always positive definite quantities regardless of the sign of the SFG intensity change.) This signal reversal results from out-of-phase NR in the $t_2 = 0.1$ ps data that is absent at larger values of t_2. In Figure 9b with $t_2 = 0.1$ ps, the SFG spectrum is a NR peak and a R dip similar to Figure 3a. As the SAM molecules heat up, the dip grows smaller so the wavelength-integrated SFG signal increases. But in $t_2 > 0.1$ ps slices NR is suppressed, the SFG spectrum consists only of peaks as in Figure 3c, and flash-heating causes those peaks to lose intensity. This signal reversal phenomenon is also seen in Figure 10a. The three-oscillator FID has a rapidly varying temporal structure near $t_2 = 0$, so the SFG intensity change in the t_1 slices with $t_2 \approx 0$ flips between an increase and a decrease with small variations of t_2. The SFG signal for $t_2 = 0.1$ ps in Figure 10b just happens to be a signal increase.

6. Experiments with Narrow-Band Visible and Femtosecond Visible Pulses

To show that effects predicted by our simulation modeling can be observed experimentally, we present some preliminary data from flash-heated AT SAMs in Figures 11 and 12. In Figure 11, time-asymmetric narrow-band probe pulses were used. The peak feature near $t = 0$ is an artifact resulting from
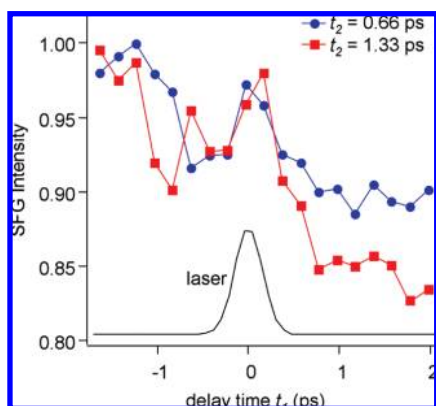
FIGURE 11. SFG intensity from an AT SAM after flash-heating to ~800 °C using a time-asymmetric NBVIS pulse to suppress the nonresonant background. The curve denoted "laser" is the cross-correlation between the flash-heating and BBIR pulses. The feature near $t = 0$ is an artifact used as fiducial time zero. As t_2 is increased, the time when the SFG intensity first rises off the baseline shifts to earlier values of t_1.
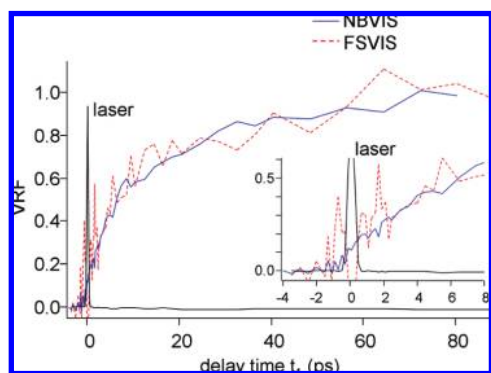

FIGURE 12. Vibrational response function (VRF) from an AT SAM after flash-heating to ~800 °C using either FSVIS or picosecond NBVIS pulses. The curve marked "laser" is the cross-correlation of the flash-heating and BBIR pulses. As shown in the inset, the initial rise of the VRF off the baseline was more abrupt when FSVIS pulses were used, indicating an improvement in time resolution.

interactions among SFG and flash-heating pulses, and it serves as a zero-time fiducial marker.[21,24] As the t_2 delay is increased, one can easily see how the rise off the baseline moves toward earlier t_1 values as t_2 increases. In Figure 12 we compare femtosecond and picosecond narrow-band probe pulses at a fixed t_2 large enough for NR suppression. The inset exploding the shorter-time part of the VRFs shows that the rise off the baseline is more abrupt with femtosecond pulses, so the overall time resolution has improved.

7. Summary and Conclusions

SFG is a powerful method for probing ultrafast processes at surfaces and interfaces, despite the sensitivity issues posed by the small number of interfacial molecules. In contrast to an ordinary pump−probe measurement with two pulses and a

single delay time, an ultrafast SFG experiment has three pulses, one pump pulse and two probe pulses, and two delay times. Such SFG experiments are both two-dimensional and coherent. Using examples drawn from studies of flash-heating measurements of thermal transport through interfacial molecules, we first described results obtained in the simpler case where the visible probe pulse is effectively infinite in duration, with only a single delay-time parameter. The problems with this method stem from the NR background and time resolution limited not by laser parameters (which can always be improved) but by intrinsic molecular dephasing rates. We described, simulated and presented results from measurements where the visible pulse was either a single-sided picosecond pulse or a femtosecond pulse. We showed we could suppress the NR signal and achieve femtosecond time resolution of the probing process, but always with a trade-off. When the NR signals were suppressed by delaying the visible pulse by a time t_2, the molecular response also shifted in time, so an accurate measurement of the molecular response required an additional knowledge of t_2. With a femtosecond visible pulse, better time resolution could result, but the ability to resolve individual vibrational transitions may be lost. In all these situations unique information about the ultrafast dynamical behavior of interfacial molecules can be obtained.

BIOGRAPHICAL INFORMATION

Jeffrey A. Carter was born in 1983 in Roanoke, Virginia. After receiving a B.S. degree from Virginia Tech in 2005, he joined the group of Prof. Dana D. Dlott. He is a Merck graduate fellow in physical chemistry.

Zhaohui Wang received a B.S. degree in chemistry in 1991, an M.S. in physical chemistry in 1994 from Fudan University, and a Ph.D. degree in 1997 in physical chemistry from the Institute of Chemistry, Chinese Academy of Sciences. He was a postdoctoral associate in Israel from 1998 to 2000 under Prof. Sanford Ruhman at Hebrew University. He is now a visiting scientist with Prof. Dana D. Dlott. Dr. Wang's research interests are in the areas of femtosecond vibrational spectroscopy, vibrational dynamics in condensed phases and energy transport at surfaces and interfaces.

Dana D. Dlott was born in 1952 in Los Angeles, CA. He received an A.B. in Chemistry from Columbia University in 1974 and a Ph.D. in Chemistry from Stanford University in 1979. He is presently William H. and Janet G. Lycan Professor of Chemistry in the School of Chemical Sciences at the University of Illinois. Prof. Dlott's research interests involve ultrafast molecular processes in materials, including heat transfer and shock compression.

REFERENCES

1 Shen, Y. R. Surfaces probed by nonlinear optics. *Surf. Sci.* **1994**, *299/300*, 551–562.

2 Chen, Z.; Shen, Y. R.; Somorjai, G. A. Studies of polymer surfaces by sum frequency generation vibrational spectroscopy. *Annu. Rev. Phys. Chem.* **2002**, *53*, 437–465.

3 Williams, C. T.; Beattie, D. A. Probing buried interfaces with non-linear optical spectroscopy. *Surf. Sci.* **2001**, *500*, 545–576.

4 Richmond, G. L. Molecular bonding and interactions at aqueous surfaces as probed by vibrational sum frequency spectroscopy. *Chem. Rev.* **2002**, *102*, 2693–2724.

5 Vidal, F.; Tadjeddine, A. Sum-frequency generation spectroscopy of interfaces. *Rep. Prog. Phys.* **2005**, *68*, 1095–1127.

6 Richter, L. J.; Petralli-Mallow, T. P.; Stephenson, J. C. Vibrationally resolved sum-frequency generation with broad-bandwidth infrared pulses. *Opt. Lett.* **1998**, *23*, 1594–1596.

7 van der Ham, E. W. M.; Vrehen, Q. H. F.; Eliel, E. R. Self-dispersive sum-frequency generation at interfaces. *Opt. Lett.* **1996**, *21*, 1448–1450.

8 van der Ham, E. W. M.; Vrehen, Q. H. F.; Eliel, E. R. High-resolution sum-frequency spectra using broadband laser sources. *Surf. Sci.* **1996**, *368*, 96–101.

9 Lagutchev, A.; Hambir, S. A.; Dlott, D. D. Nonresonant background suppression in broadband vibrational sum-frequency generation spectroscopy. *J. Phys. Chem. C* **2007**, *111*, 13645–13647.

10 Shen, Y. R. *The Principles of Nonlinear Optics*; Wiley: New York, 1984.

11 Harris, A. L.; Chidsey, C. E. D.; Levinos, N. J.; Loiacono, D. N. Monolayer vibrational spectroscopy by infrared-visible sum generation at metal and semiconductor surfaces. *Chem. Phys. Lett.* **1987**, *141*, 350–356.

12 Arnolds, H.; King, D. A.; Lane, I. M. Inducing non-adiabatic effects through coadsorption: CO+NO on iridium. *Chem. Phys.* **2008**, *350*, 94–103.

13 Lane, I. M.; King, D. A.; Liu, Z.-P.; Arnolds, H. Real-time observation of nonadiabatic surface dynamics: The first picosecond in the dissociation of NO on iridium. *Phys. Rev. Lett.* **2006**, *97*, 186105-1–186105-4.

14 Hess, C.; Bonn, M.; Funk, S.; Wolf, M. Hot-band excitation of CO chemisorbed on Ru(001) studied with broadband-IR sum-frequency generation. *Chem. Phys. Lett.* **2000**, *325*, 139–145.

15 Hess, C.; Wolf, M.; Bonn, M. Direct observation of vibrational energy delocalization on surfaces: CO on Ru(001). *Phys. Rev. Lett.* **2000**, *85*, 4341–4344.

16 Bonn, M.; Hess, C.; Wolf, M. The dynamics of vibrational excitations on surfaces: CO on Ru(001). *J. Chem. Phys.* **2001**, *115*, 7725–7735.

17 Ghosh, A.; Smits, M.; Sovago, M.; Bredenbeck, J.; Müller, M.; Bonn, M. Ultrafast vibrational dynamics of interfacial water. *Chem. Phys.* **2008**, *350*, 23–30.

18 Sovago, M.; Campen, R. K.; Wurpel, G. W. H.; Muller, M.; Bakker, H. J.; Bonn, M. Vibrational response of hydrogen-bonded interfacial water is dominated by intramolecular coupling. *Phys. Rev. Lett.* **2008**, *100*, 173901-1–173901-4.

19 Lagutchev, A. S.; Patterson, J. E.; Huang, W.; Dlott, D. D. Ultrafast Dynamics of Self-Assembled Monolayers Under Shock Compression: Effects of molecular and substrate structure. *J. Phys. Chem. B* **2005**, *109*, 5033–5044.

20 Patterson, J. E.; Lagutchev, A. S.; Huang, W.; Dlott, D. D. Ultrafast dynamics of shock compression of molecular monolayers. *Phys. Rev. Lett.* **2005**, *94*, 015501-1–015501-4.

21 Wang, Z.; Carter, J. A.; Lagutchev, A.; Koh, Y. K.; Seong, N.-H.; Cahill, D. G.; Dlott, D. D. Ultrafast flash thermal conductance of molecular chains. *Science* **2007**, *317*, 787–790.

22 Pang, Y.; Deàk, J. C.; Huang, W.; Lagutchev, A.; Pakoulev, A.; Patterson, J. E.; Sechler, T. D.; Wang, Z.; Dlott, D. D. Vibrational energy in molecules probed with high time and space resolution. *Int. Rev. Phys. Chem.* **2007**, *26*, 223–248.

23 Carter, J. A.; Wang, Z.; Dlott, D. D. Spatially resolved vibrational energy transfer in molecular monolayers. *J. Phys. Chem. A* **2008**, *112*, 3523–3529.

24 Wang, Z.; Cahill, D. G.; Carter, J. A.; Koh, Y. K.; Lagutchev, A.; Seong, N.-H.; Dlott, D. D. Ultrafast dynamics of heat flow across molecules. *Chem. Phys.* **2008**, *350*, 31–44.

25 McCamant, D. W.; Kukura, P.; Mathies, R. A. Femtosecond time-resolved stimulated Raman spectroscopy: Application to the ultrafast internal conversion in beta-carotene. *J. Phys. Chem. A* **2003**, *107*, 8208–8214.

26 Segal, D.; Nitzan, A. Heating in current carrying molecular junctions. *J. Chem. Phys.* **2002**, *117*, 3915–3927.

27 Segal, D.; Nitzan, A.; Hänggi, P. Thermal conductance through molecular wires. *J. Chem. Phys.* **2003**, *119*, 6840–6855.

28 Galperin, M.; Ratner, M. A.; Nitzan, A. Molecular transport junctions: vibrational effects. *J. Phys.: Condens. Matter* **2007**, *19*, 103201-1–103201-81.

29 Bain, C. D.; Davies, P. B.; Ong, T. H.; Ward, R. N. Quantitative analysis of monolayer composition by sum-frequency vibrational spectroscopy. *Langmuir* **1991**, *7*, 1563–1566.

30 Roke, R.; Kleyn, A. W.; Bonn, M. Time- vs. frequency-domain femtosecond surface sum frequency generation. *Chem. Phys. Lett.* **2003**, *370*, 227–232.

31 Shen, Y. R. Surface properties probed by second-harmonic and sum-frequency generation. *Nature (London)* **1989**, *337*, 519–525.

32 Wynne, K.; Hochstrasser, R. M. The theory of ultrafast vibrational spectroscopy. *Chem. Phys.* **1995**, *193*, 211–236.

33 Mukamel, S. *Principles of Nonlinear Optical Spectroscopy*; Oxford University Press: New York, 1995.

34 Lu, G. Q.; Lagutchev, A.; Dlott, D. D.; Wieckowski, A. Quantitative vibrational sum-frequency generation spectroscopy of thin layer electrochemistry: CO on a Pt electrode. *Surf. Sci.* **2005**, *585*, 3–16.

35 McGuire, J. A.; Beck, W.; Wei, X.; Shen, Y. R. Fourier-transform sum-frequency surface vibrational spectroscopy with femtosecond pulses. *Opt. Lett.* **1999**, *24*, 1877–1879.

36 Bordenyuk, A. N.; Jayathilake, H. D.; Benderskii, A. V. Coherent vibrational quantum beats as a probe of Langmuir—Blodgett monolayers. *J. Phys. Chem. B* **2005**, *109*, 15941–15949.

37 Lagutchev, A.; Lu, G. Q.; Takeshita, T.; Dlott, D. D.; Wieckowski, A. Vibrational sum frequency generation studies of the $(2 \times 2) \rightarrow (\sqrt{19} \times \sqrt{19})$ phase transition of CO on Pt(111) electrodes. *J. Chem. Phys.* **2006**, *125*, 154705-1–154705-10.

38 Brorson, S. D.; Fujimoto, J. G.; Ippen, E. P. Femtosecond electronic heat-transport dynamics in thin gold films. *Phys. Rev. Lett.* **1987**, *59*, 1962–1965.

39 Hohlfeld, J.; Wellershoff, S.-S.; Güdde, J.; Conrad, U.; Jähnke, V.; Matthias, E. Electron and lattice dynamics following optical excitation of metals. *Chem. Phys.* **2000**, *251*, 237–258.

40 Cahill, D. G. Analysis of heat flow in layered structures for time-domain thermoreflectance. *Rev. Sci. Instrum.* **2004**, *75*, 5119–5122.

41 Scouler, W. J. Temperature-modulated reflectance of gold from 2 to 10 eV. *Phys. Rev. Lett.* **1967**, *18*, 445–448.

42 Jiang, L.; Tsai, H.-L. Improved two-temperature model and its application in ultrashort laser heating of metal films. *J. Heat Transfer* **2005**, *127*, 1167–1173.